CHALMERS
UNIVERSITY OF TECHNOLOGY

Implementation of the Neoclassical Tearing Mode model in the European Transport Simulator integrated modelling workflow

Master's thesis in Physics

CHARBEL NEMER

DEPARTMENT OF SPACE, EARTH AND ENVIRONMENT

CHALMERS UNIVERSITY OF TECHNOLOGY
Gothenburg, Sweden 2025
www.chalmers.se

Master's thesis 2025

Implementation of the Neoclassical Tearing Mode model in the European Transport Simulator integrated modelling workflow

CHARBEL NEMER

CHALMERS
UNIVERSITY OF TECHNOLOGY

Department of Space, Earth and Environment
Division of Astronomy and Plasma Physics
Plasma Physics and Fusion Energy
Chalmers University of Technology
Gothenburg, Sweden 2025

Implementation of the Neoclassical Tearing Mode model in the European Transport Simulator integrated modelling workflow
CHARBEL NEMER

Supervisor: Dmytro Yadykin, Space Earth and Environment
Examiner: Pär Strand, Space Earth and Environment

Master's Thesis 2025
Department of Space Earth and Environment
Division of Astronomy and Plasma Physics
Plasma Physics and Fusion Energy
Chalmers University of Technology
SE-412 96 Gothenburg
Telephone +46 31 772 1000

Typeset in LaTeX
Printed by Chalmers Reproservice
Gothenburg, Sweden 2025

Implementation of the Neoclassical Tearing Mode model in the European Transport Simulator integrated modelling workflow

CHARBEL NEMER
Department of Space, Earth and Environment
Chalmers University of Technology

Abstract

Neoclassical tearing modes (NTMs) are plasma instabilities that degrade performance in tokamak plasmas. This work implements a numerical calculation of the perturbed helical flux (ψ) to calculate the linear tearing stability index (Δ'_0). The implementation is done using integrated modelling workflows in the European Transport Simulator (ETS) and the High Modularity Physics Simulator (HMPS) frameworks. The large aspect ratio approximation ($a/R \ll 1$) is assumed for all calculations in this project. Simulations were done on the (3,2) and (2,1) tearing modes. The (2,1) tearing mode obtained a $\Delta'_0 = -6.43\,\mathrm{m}^{-1}$ using the cylindrical approximation and $\Delta'_0 = -7.83\,\mathrm{m}^{-1}$ using the full ψ calculation. The (3,2) mode obtained $\Delta'_0 = -11.06\,\mathrm{m}^{-1}$ with the cylindrical approximation and $\Delta'_0 = -11.55\,\mathrm{m}^{-1}$ with the full ψ calculation. The simulations show that for the plasma scenario used, the numerical integration gives lower values of the stability tearing index than the cylindrical approximation. This can possibly point to the cylindrical approximation being used as an upper limit of Δ'_0. These results also show that the tearing modes are stable for the plasma scenario used. Furthermore, the modified Rutherford equation was used to show different contributions to the NTM stability. For both (3,2) and (2,1) modes the largest contribution to stability came from the classical tearing index. The curvature term (Δ'_{GGJ}) showed a stabilising effect as well and the perturbed bootstrap current term (Δ'_{bs}) showed a destabilising effect on the NTM. For the plasma scenario used in the project the stabilising effects far outweighed the destabilising effects leading to no growth of magnetic islands.

Keywords: Neoclassical Tearing Mode, ETS, linear stability tearing index, perturbed helical flux

Acknowledgements

This project was a big undertaking for me and I would like to thank all the people that helped me see it through. My supervisor Dmytro Yadykin has been so active and helpful in this process and I can't thank him enough for his engagement with all the ups and downs I've gone through in this process. There was so much I didn't know when I started this project which he taught me and I'm very grateful for that. I would also like to extend thanks to Francesca Poli whom has been my contact at ITER. She has helped me through this project in many ways and was always open to questions and suggestions. Without these two people, this work would not have been possible. I also want to thank my examiner Pär Strand for letting me do this project and for all the nice morning meetings each week. I also want to thank Isak Larsén for all the conversations and help he has provided as we have gone through the process of writing our theses in parallel. By the same token I want to thank Pablo Arriagada Torres for being such a wonderful person to talk to. Especially when the progress was going slowly, he is a person that cheers you up very easily. Finally, I want to thank my parents, Bernadette and Abdelmassih and younger brother Georgio for being such an amazing support net. They have listened through all my complaints and all my happy moments through out this process. Having them by my side has meant more than they can know.

Charbel Nemer, Gothenburg, November 2025

List of Acronyms

Below is the list of acronyms that have been used throughout this thesis listed in alphabetical order:

DD	Data Dictionary (IMAS)
ETS	European Transport Simulator
HMPS	High Modularity Physics Simulator
IDS	Interface Data Structure
IMAS	Integrated Modelling & Analysis Suite
ITER	International Thermonuclear Experimental Reactor
JET	Joint European Torus
MHD	Magnetohydrodynamics
MMSL	Multiscale Modelling and Simulation Language
MRE	Modified Rutherford Equation
MUSCLE3	Multiscale Modelling and Simulation Library 3
NTM	Neoclassical Tearing Mode
RE	Rutherford Equation
SDCC	Science Data & Computing Center (ITER)
TM	Tearing Mode

Contents

List of Figures

List of Tables

1

Introduction

For over 70 year research on nuclear fusion has been conducted for the purpose of using fusion as a source of energy [4]. Although the phenomenon of nuclear fusion in stars has been studied for decades earlier than this. If achieved, commercial nuclear fusion would provide a sustainable and clean energy source with a minimal carbon footprint.

The challenge of creating sustained nuclear fusion in a terrestrial setting is the following. Fusion in nature occurs under extreme conditions inside stars. It requires immense amounts of pressure that is generated by the gravity of a massive object like a star. Without the large pressures and the high temperatures that exist within such a system it is very difficult to fuse atomic nuclei. Any vessel created on earth simply can not contain a fusion plasma under such conditions.

One possible solution that has been explored since early days in fusion research is magnetic confinement of plasmas. The principle of magnetic confinement is that a plasma can be contained using strong magnetic fields. Given the correct geometric configuration and strength of such fields it becomes possible to contain highly pressurized, ionized gas at high temperature.

One of the earliest reactor designs introduced was the tokamak reactor [4]. The tokamak is geometrically shaped like a torus. External coils induce electric and magnetic fields inside the tokamak. The plasma current is induced due to transformer action. The plasma acts as a secondary coli to the central solenoid. The plasma current in turn induces a poloidal magnetic field. The toroidal magnetic field is induced by external coils. The poloidal and toroidal magnetic fields are the basis for confining a plasma in a tokamak [1].

Magnetic confinement inside the tokamak is a difficult technical challenge to achieve. Partly due to the amplitude of the magnetic fields that have to be generated. But also due to the fact that there are plasma instabilities that can occur that often promote the transport of heat, energy and particles away from the centre of the reactor. Such instabilities lead to worse performance of the reactor and thus less energy output. In the worst cases the plasma can degrade to the point where no fusion occurs.

Plasma instabilities are in general perturbations of plasma quantities that grow with time. Perturbations can be caused by a multitude of factors such as fluctuations in the electric and magnetic fields. When instabilities disturb the equilibrium state of the plasma the performance is reduced. That is why understanding and mitigating plasma instabilities is an important part of fusion research.

A plasma phenomenon of interest for this work is magnetic reconnection. That is when magnetic field lines within a plasma break and reconnect due to magnetic diffusion. In the context of tokamak plasmas magnetic reconnection can promote instabilities to grow and disrupt the equilibrium state. This usually results in enhanced particle and energy transport which degrades plasma confinement and performance.

This project focuses on the numerical simulations related to the linear tearing mode (TM) and the neoclassical tearing mode (NTM). Tearing modes are resistive instabilities induced by perturbations and occur on special regions in the plasma called tearing layers. Magnetic reconnection occur across the tearing layer, making it an important phenomenon to study. The difference between TMs and NTMs is that the TMs are driven by the pre existing radial current gradient while NTMs are driven by additional bootstrap current effects. When tearing modes are present the reconnecting magnetic field lines change their topology around the tearing layer. The field lines look like islands which is why they are called magnetic islands. The magnetic islands flatten pressure and flux profiles which promotes the transport of energy and particles from the interior of the tokamak to the edges. The understanding of how these magnetic islands grow in time and how to suppress them is important in order to achieve good plasma performance.

The NTM begins with a seed island at a tearing layer within the confinement vessel. Tearing layers occur on rational surfaces where the the safety factor takes on a rational value. Due to the radial pressure gradient there is free energy that the tearing mode can use to grow in time.

This project used integrated modelling to simulate the tearing modes described above. Integrated modelling is systematic approach to creating and running simulations. The European Transport Simulator (ETS) is a workflow where the NTMs are a part of the physics being modelled. The Integrated Modelling & Analysis Suite (IMAS) framework was used to write code for and run simulations of TMs and NTMs in different plasma scenarios. The workflow structure of this approach allowed for development of the code in a real scientific modelling setting.

The development and simulations in this project were done using the integrated modelling workflow developed in the EU framework and in collaboration with the International Thermonuclear Experimental Reactor (ITER). The ITER Science Data & Computing Center (SDCC) was used to access remote computing resources where code was developed and simulations were ran. The ETS was used to run simulations of the linear tearing modes and check the how the magnetic islands behave in stable plasma scenarios. The implementations done were also tested in a framework currently in development called the High Modularity Physics Simulator (HMPS).

2

Theory

2.1 Magnetohydrodynamics

The magnetohydrodynamic (MHD) model of plasmas will be the basis of simulations in this project. The reason being that much of plasma modelling is done through the lens of MHD. The single fluid hydrodynamic model of plasmas describes macroscopic properties of the plasma which makes simulations more approachable as opposed to kinetic models of plasmas which take a more microscopic approach. Using the MHD model allows for simplifications in computation. The drawback of this approach is that macroscopic properties such as pressure and particle density describe the large scale behaviour of a plasma but not the exact behaviour of every individual particle. When this approach is insufficient it can be used in tandem with other approaches such as kinetic models [7].

The equations governing the resistive MHD plasma are given by

$$\frac{\partial \rho}{\partial t} + \nabla \cdot (\rho \mathbf{v}) = 0, \tag{2.1}$$

$$\frac{d}{dt}\left(\frac{p}{\rho^\gamma}\right) = 0, \tag{2.2}$$

$$\rho \frac{d\mathbf{v}}{dt} = \mathbf{j} \times \mathbf{B} - \nabla p, \tag{2.3}$$

$$\nabla \times \mathbf{B} = \mu_0 \mathbf{j}, \tag{2.4}$$

$$\nabla \times \mathbf{E} = -\frac{\partial \mathbf{B}}{\partial t}, \tag{2.5}$$

$$\nabla \cdot \mathbf{B} = 0, \tag{2.6}$$

$$\mathbf{E} + \mathbf{v} \times \mathbf{B} = \eta \mathbf{j}. \tag{2.7}$$

These equations describe the dynamics of a single electrically conducting fluid. The first equation (2.1) is the mass continuity equation. It relates the change in mass density of the plasma (ρ) with respect to time to the divergence of the mass flux of the plasma ($\rho\mathbf{v}$) where $\mathbf{v}$ is the velocity field of the plasma. Next is equation (2.2) which is the adiabatic equation of state. It follows directly from the ideal gas law

and applies the assumption that processes in MHD do not exchange heat with their surrounding environment. Next is equation (2.3) which the equation of motion. It relates the acceleration of the plasma to the forces acting on it. The left hand side describes how the plasma accelerates in term of the plasma mass density. The first term on the right hand side being the Lorentz force given by the term $\mathbf{j} \times \mathbf{B}$ and the second term being the force that appears due to the plasma pressure. Equation (2.3) is important in the context of MHD since it connects the fluid part of the model $(\rho, \boldsymbol{v})$ to the electromagnetic part $(\mathbf{j}, \mathbf{B})$. The equations (2.4), (2.5) and (2.6) are Maxwell equations that relate the electric field $(\mathbf{E})$ to the magnetic field $(\mathbf{B})$. And the magnetic field to the plasma current $(\mathbf{j})$. Finally, equation (2.7) is the resistive Ohm's law. In the ideal MHD case resistivity $\eta \approx 0$ but this is not always true and becomes relevant later on in this project [7].

2.2 MHD equilibrium in tokamaks

The plasma equilibrium state is important for the understanding of how instabilities effect plasma performance. In this project equilibrium quantities will be used as input for different calculations in the simulations. From the MHD equations (2.1)-(2.7) the momentum equation (2.3) is especially important for the equilibrium. A static equilibrium is defined by the plasma being in force balance. This means that the acceleration term in the equation of motion is zero and the momentum equation becomes

$$\mathbf{j} \times \mathbf{B} = \nabla p. \tag{2.8}$$

As can be seen from equation (2.8), the force on the plasma from the kinetic pressure gradient is completely balanced by the Lorentz force.

2.2.1 Coordinate systems

In tokamak fusion research there are many coordinate conventions used. Therefore it is important that one is aware of the system of coordinates begin used for any given calculation and how to convert between different conventions.

The tokamak geometry is often characterized by a cylindrical coordinate system used to describe toroidal geometry. This system has one basis vector along the direction of the major radius $(\hat{\boldsymbol{R}})$, one basis vector that goes through the centre of the torus $(\hat{\boldsymbol{Z}})$ and the third basis vector that follows the toroidal angle $(\hat{\boldsymbol{\phi}})$.

The coordinate system in figure 2.1 is well defined and is often used but for some applications, it can be less convenient. Therefore, it can be more useful to define different systems depending on the application. The Shafranov coordinates [9] can for instance be defined in relation to the cylindrical system above according to

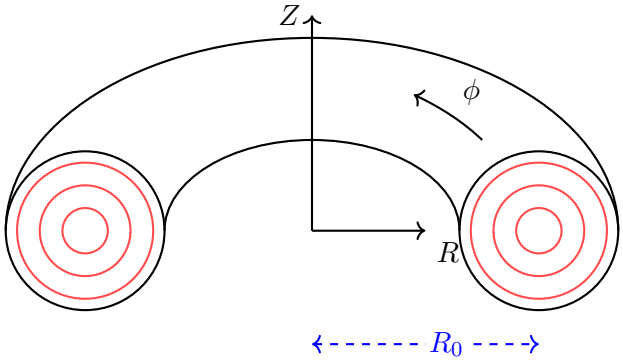

Figure 2.1: Toroidal description of tokamak geometry. The right handed system is (R, ϕ, Z). The major radius is denoted by R_0

$$\begin{aligned} R &= R_0 + r\cos(\theta) - D(r), \\ z &= r\sin(\theta), \\ \phi &= -\varphi. \end{aligned} \tag{2.9}$$

The new coordinate system contains the minor radius r, the poloidal angle θ and the toroidal angle φ. This coordinate system is centred at the magnetic axis and is more suitable for equilibrium calculations. The quantity $D(r)$ corresponds to the Shafranov shift and will not be explicitly considered in this project. For large aspect ratio tokamaks $R/a \gg 1$ this shift is small [9].

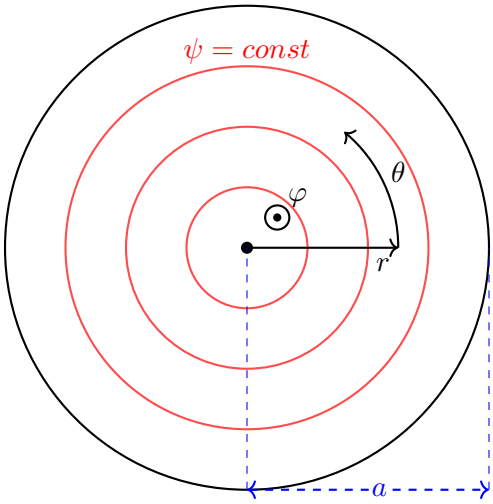

Figure 2.2: Tokamak poloidal cross section schematic showing the Shafranov system centred at the magnetic axis. The right handed system is (r, θ, φ). The concentric rings represent surfaces of constant flux. The minor radius of the tokamak is denoted by a.

The Shafranov system in figure 2.2 can be related to flux coordinate systems. These systems map the minor radius to a magnetic flux. An assumption made is that the reference magnetic flux function is monotonic as a function of the minor radius. The reference flux function can be defined in several ways with different signs and normalizations which gives rise to different coordinate conventions.

An important quantity when working with flux coordinates is the poloidal flux. It is given by

$$\Psi_{\text{pol}} = -\sigma_{Bp} \int \mathbf{B} \cdot d\mathbf{S}_p. \tag{2.10}$$

Given a point (R_1, Z_1) the surface element $d\mathbf{S}_p$ is defined as the disk $R \leq R_1, Z = Z_1$. The orientation of this disk depends on the choice of right handed system. This is encoded through the parameter σ_{Bp} [14]. The reference flux can thus be defined in terms of the poloidal flux as

$$\psi_{\text{ref}} = \frac{\Psi_{\text{pol}}}{(2\pi)^{(1-e_{Bp})}} \tag{2.11}$$

where $e_{Bp} = 0$ or 1 depending on whether the poloidal flux already normalized by 2π or not.

The tokamak system of interest is the large aspect ratio tokamak which can be defined through the inverse aspect ratio according to

$$\varepsilon \equiv \frac{a}{R} \ll 1. \tag{2.12}$$

The force balance equation (2.8) can now be expressed in terms of the Shafranov coordinates as

$$\mathbf{j} \times \mathbf{B} = \nabla p \Leftrightarrow \tag{2.13}$$

$$(j_\theta B_\phi - B_\theta j_\phi)\hat{\mathbf{r}} = \frac{\partial p}{\partial r}\hat{\mathbf{r}}, \tag{2.14}$$

$$(j_\phi B_r - B_\phi j_r)\hat{\boldsymbol{\theta}} = \frac{\partial p}{\partial \theta}\hat{\boldsymbol{\theta}}, \tag{2.15}$$

$$(j_r B_\theta - B_r j_\theta)\hat{\boldsymbol{\varphi}} = \frac{\partial p}{\partial \phi}\hat{\boldsymbol{\varphi}}. \tag{2.16}$$

$$\tag{2.17}$$

An important note is that the quantities $\mathbf{j}$, $\mathbf{B}$ and ∇p are flux functions [17]. This means they can be expressed in terms flux functions such as the poloidal flux Ψ_{pol}. These functions have the property of being constant on the magnetic surfaces.

2.2.2 Safety factor

An important quantity in the study of tokamak plasmas is the safety factor generally denoted q. The safety factor is a measure of how the magnetic field lines in a tokamak rotate in the poloidal plane as one travels along the toroidal direction. In an axisymmetric equilibrium the magnetic field lines move in a helical path around the torus [17]. The safety factor q is defined by the total change in toroidal angle $\Delta\phi$ for each poloidal turn $\theta = 2\pi$ a magnetic field line travels. This is expressed as

$$q \equiv \frac{\Delta\phi}{2\pi}. \tag{2.18}$$

We turn to the defining equation of the magnetic field lines given by

$$\frac{\mathrm{d}\mathbf{r}}{\mathrm{d}s} = \frac{\mathbf{B}}{|\mathbf{B}|}. \tag{2.19}$$

In the large aspect ratio, axisymmetric tokamak equilibrium where $\mathbf{B}_r = 0$ the following relations are obtained:

$$\frac{R\mathrm{d}\phi}{\mathrm{d}s} = \frac{B_\phi}{B}, \tag{2.20}$$

$$\frac{r\mathrm{d}\theta}{\mathrm{d}s} = \frac{B_\theta}{B}, \tag{2.21}$$

which can be combined into

$$R\frac{\mathrm{d}\phi}{r\mathrm{d}\theta} = \frac{B_\phi}{B_\theta}. \tag{2.22}$$

From this equation (2.22) and equation (2.18) the following continuos expression for q can be written:

$$q = \oint \frac{\mathrm{d}\phi}{2\pi} = \frac{1}{2\pi}\oint \frac{1}{R}\frac{B_\phi}{B_\theta} r\mathrm{d}\theta. \tag{2.23}$$

The safety factor is a flux function, meaning it can be expressed in terms of the poloidal or toroidal flux ($q = q(\psi)$). In the large aspect ratio approximation of a cylindrical tokamak ($R \approx R_0$) the integration of equation (2.23) gives

$$q = \frac{rB_\phi}{R_0 B_\theta}. \tag{2.24}$$

Rational surfaces are surfaces of constant flux where the safety factor takes a value of the form $q = m/n$. Here, m is the poloidal winding number of the magnetic field and n is the toroidal winding number. These surfaces are especially interesting to consider since the tearing modes appear on them.

2.2.3 Quantity orderings

To study the equilibrium in greater detail and understand the effects of perturbations we must express the quantities in in terms of the inverse aspect ratio ε. We begin with expressing the equilibrium quantities in tokamaks and the quantity orderings that are appropriate given the assumption made in equation (2.12).

Several field quantities are important when considering the tokamak equilibrium plasma. We consider first the magnetic fields. External coils wound around the poloidal plane of the tokamak give rise to the toroidal magnetic field [17]. By using Ampère's circuit law and integrating over a line segment along a closed toroidal loop one obtains

$$\oint_C \mathbf{B} \cdot \mathbf{dl} = \mu_0 I, \tag{2.25}$$

$$\Rightarrow 2\pi R B_\phi = \mu_0 I, \tag{2.26}$$

$$\Leftrightarrow B_\phi \propto \frac{I}{R}. \tag{2.27}$$

Here, R is the coordinate along the major radius and I is the current passing through a closed circuit of radius R. It is true in tokamak equilibria that the toroidal magnetic field is much larger in amplitude than the poloidal magnetic field. This is expressed as

$$\left|\frac{B_\theta}{B_\phi}\right| \ll 1. \tag{2.28}$$

In equilibrium, the radial magnetic field B_r is essentially zero since there are no external currents that provide an equilibrium magnetic field in the radial direction. The poloidal magnetic field is created in part due to the bootstrap current of the plasma and the central solenoid [17]. The largest field here is the toroidal magnetic field. This is reflected in the condition 2.28.

Now, let's express these quantities in the large aspect ratio limit of tokamaks. This limit is used throughout this project. The quantities of interest are the following. The toroidal magnetic field ($B_{\phi 0}$), the poloidal magnetic field ($B_{\theta 0}$), the toroidal current ($j_{\phi 0}$) and the poloidal current ($j_{\theta 0}$).

Starting with the toroidal equilibrium field, as seen from equation (2.27) it can be expressed as $B_\phi = B_{\phi 0} R_0 / R$ where $B_{\phi 0}$ is the magnetic field at the magnetic axis.

This holds for a perfectly circular tokamak cross section. When geometric properties of a realistic tokamak like elongation and triangularity are included the equilibrium toroidal field obtains a correction term of order $\mathcal{O}(\varepsilon^2)$. The equilibrium toroidal magnetic field becomes

$$B_\phi = B_{\phi 0}\frac{R_0}{R}(1 + \mathcal{O}(\varepsilon^2)). \tag{2.29}$$

Using appropriate assumptions regarding the different fields and current densities, we obtain quantity ordering for the equilibrium in a tokamak. First, we consider the expression of the safety factor given by equation (2.24). This expression directly relates the toroidal field to the poloidal field. The safety factor changes on the order $q(r) \sim \mathcal{O}(1)$ along the minor radius [11]. This expression yields the following ordering for B_θ,

$$B_\theta = \frac{rB_\phi}{R_0 q} \sim \frac{rB_{\phi 0}R_0/R}{R_0} \sim \varepsilon B_{\phi 0}. \tag{2.30}$$

Next we consider the toroidal current density which can be obtained via Ampère's law as follows:

$$(\nabla \times \mathbf{B})_\theta = \mu_0 j_\phi \Leftrightarrow \frac{1}{r}\left(\frac{\partial}{\partial r}(rB_\theta) - \frac{\partial}{\partial \theta}B_r\right) = \mu_0 j_\phi. \tag{2.31}$$

The assumption of axisymmetric equilibrium ($B_r = 0$) together with equation (2.30) give the toroidal current density ordering

$$j_\phi \sim \frac{1}{\mu_0}\frac{1}{r}\frac{\partial}{\partial r}\left(r\varepsilon B_{\phi 0}\right) \sim \frac{\varepsilon B_{\phi 0}}{\mu_0 a}. \tag{2.32}$$

Here $r \sim a$ since this is the scale of the minor radius. Next we consider the pressure ordering. The fraction of the fluid pressure to the magnetic pressure (β) is given by

$$\beta = \frac{p}{|\mathbf{B}|^2/2\mu_0}. \tag{2.33}$$

Here β is assumed to be of order $\mathcal{O}(\varepsilon^2)$. The pressure ordering can thus be written as

$$p \sim \frac{\varepsilon^2 B_{\phi 0}^2}{\mu_0}. \tag{2.34}$$

Now we can express the radial force balance equation (2.8) in combination with Ampère's law (2.4). This is done in the radial direction and we obtain

$$\mu_0 \frac{\mathrm{d}p}{\mathrm{d}r} = \frac{B_\theta}{r}\frac{\mathrm{d}}{\mathrm{d}r}(rB_\theta) + B_\phi \frac{\mathrm{d}B_\phi}{\mathrm{d}r}. \tag{2.35}$$

Using the ordering $\frac{\mathrm{d}p}{\mathrm{d}r} \sim p/a$ we are now able to express the ordering of the quantity $\frac{\mathrm{d}B_\phi}{\mathrm{d}r}$. Looking at the ordering of each term we find

$$\frac{\mu_0}{B_\phi}\frac{\mathrm{d}p}{\mathrm{d}r} \sim \frac{\mu_0}{B_{\phi 0}}\frac{\varepsilon^2 B_{\phi 0}^2}{\mu_0 a} \sim \frac{\varepsilon^2 B_{\phi 0}}{a}, \tag{2.36}$$

$$\frac{B_\theta}{B_\phi r}\frac{\mathrm{d}}{\mathrm{d}r}(rB_\theta) \sim \frac{\varepsilon}{a}\left(B_\theta + r\frac{\mathrm{d}B_\theta}{\mathrm{d}r}\right) \sim \frac{\varepsilon^2 B_{\phi 0}}{a}. \tag{2.37}$$

Above, the fact that $\frac{\mathrm{d}\varepsilon}{\mathrm{d}r} \sim \frac{\varepsilon}{a}$ was used which can be shown by differentiating the local aspect ratio defined by $\varepsilon(r) = \frac{r}{R_0 + r}$ with respect to r. This shows that

$$\frac{\mathrm{d}B_\phi}{\mathrm{d}r} \sim \frac{\varepsilon^2 B_{\phi 0}}{a}. \tag{2.38}$$

From Ampère's law we have

$$\mu_0 j_\theta = -\frac{\mathrm{d}B_\phi}{\mathrm{d}r} \tag{2.39}$$

which we have now shown to have the ordering

$$j_\theta \sim \frac{\varepsilon^2 B_{\phi 0}}{\mu_0 a} \sim \varepsilon j_\phi. \tag{2.40}$$

When it comes to the perturbed quantities, the following orderings are assumed in this situation [17]:

$$B_{\phi 1} \sim \varepsilon B_{r1} \sim \varepsilon B_{\theta 1}, \tag{2.41}$$

$$j_{r1} \sim j_{\theta 1} \sim \varepsilon j_{\phi 1}. \tag{2.42}$$

In summary, the equilibrium quantities are ordered as follows:

$$B_\phi \sim B_{\phi 0}\left(1+\mathcal{O}(\varepsilon^2)\right), \tag{2.43}$$

$$B_\theta \sim \varepsilon B_{\phi 0}, \tag{2.44}$$

$$j_\phi \sim \varepsilon \frac{B_{\phi 0}}{\mu_0 a}, \tag{2.45}$$

$$j_\theta \sim \varepsilon j_\phi. \tag{2.46}$$

2.2.4 Ideal MHD equilibrium

There are two types of MHD equilibrium of interest for this project. The first is the ideal MHD equilibrium. It is characterised by the fact that plasma resistivity is negligible which modifies equation (2.7) to

$$\mathbf{E} + \mathbf{v} \times \mathbf{B} = 0. \tag{2.47}$$

It is a well known result that equation (2.47) implies that the magnetic field lines are frozen in the plasma [17]. This can be expressed as

$$\frac{\mathrm{D}\Phi}{\mathrm{D}t} = 0 \tag{2.48}$$

where Φ is the total magnetic flux and the derivative is the convective derivative.

This plasma configuration does not permit instabilities like the NTM to arise since there is no way for the magnetic topology to change. Although there are instabilities such as the kink instability which can still occur in the ideal plasma.

2.2.5 Resistive MHD equilibrium

The tearing mode instability becomes relevant in scenarios where the equation (2.47) does not hold as a valid approximation. This can happen when the plasma is in static equilibrium. This reduces Ohm's law (2.7) to

$$\mathbf{E} \approx \eta \mathbf{j} \tag{2.49}$$

which can be re-written using Faraday's law of induction and Ampère's law to the magnetic diffusion equation

$$\frac{\partial \mathbf{B}}{\partial t} = \frac{\eta}{\mu_0}\nabla^2 \mathbf{B}. \tag{2.50}$$

This equation allows for the magnetic topology to change in special regions which will be described more later on [3].

2.2.6 Magnetic reconnection

In the ideal plasma, the magnetic flux is conserved which implies that the field lines are "frozen" into the plasma. When plasma resistivity becomes relevant this is no longer true. The magnetic field can now diffuse which leads to reconnection at rational flux surfaces where $q(r) = m/n$. Magnetic reconnection can result structures that contain field lines which close in on them selves. An illustration of such a structure is given in figure 2.3.

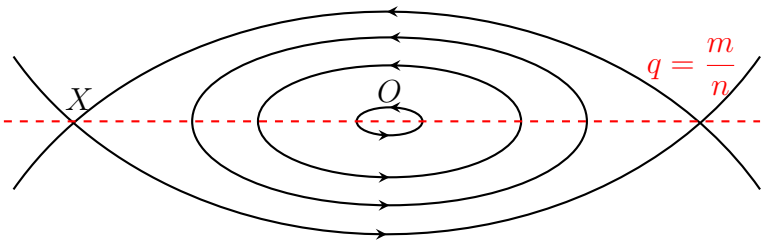

Figure 2.3: Reconnecting surface where magnetic island forms. The island has its magnetic axis at the O-point. The magnetic field lines reconnect at the X points located at the edges of the island.

The reconnection regions form islands with their own magnetic axis. The field lines on the interior of the magnetic island form closed loops. The centre of this region is usually named the O-point. The boundary of the island forms what is called the "separatrix". The X-points is where the reconnecting field lines meet which is illustrated in figure 2.3.

The property of interest in this project is the time evolution of the island width. An expression for the width can be derived by applying equation (2.19) in the vicinity of the resonant surface [17]. The width can be expressed as

$$w = 4\left(\frac{rq\hat{B}_r}{mq'B_\theta}\right)_s^{1/2}. \tag{2.51}$$

Here, q is the safety factor at the resonant surface and q' is it's radial derivative, m is the poloidal mode number of the perturbed field at the resonant surface and B_θ is the equilibrium poloidal field at r_s. To arrive at this expression one assumes that the amplitude of the perturbed magnetic field is constant across the island width. This amplitude is denoted by $\hat{B}_r$.

2.3 Linear Stability

An important property of MHD equilibrium is how stable it is. In this context, linear stability can be characterized in the following way. Consider a plasma quantity

$Q(\mathbf{r}, t)$. This is assumed to be linearisable into an equilibrium quantity $Q_0(\mathbf{r})$ and a small perturbation given by $Q_1(\mathbf{r}, t)$. We thus have

$$Q(\mathbf{r}, t) = Q_0(\mathbf{r}) + Q_1(\mathbf{r}, t)$$

where the condition

$$\left|\frac{Q_1}{Q_0}\right| \ll 1$$

generally holds. An equilibrium is considered linearly stable if $Q_1(\mathbf{r}, t) \to 0$ as $t \to \infty$, and unstable if $Q_1(\mathbf{r}, t) \to \infty$ as $t \to \infty$ [7].

2.3.1 Instability drivers

Plasma instabilities need free energy in order to form. Due to the fact that resistive instabilities change the magnetic topology of the system energy has to be exerted on the plasma in order to change the equilibrium state. Free energy can often be found in different quantity gradients. Examples of such gradients are current gradients, pressure gradients and temperature gradients. In the case of tearing modes in tokamak plasmas, the main driver is often the equilibrium current gradient. This current density gradient in combination with the magnetic diffusion that happens during reconnection drives tearing modes to grow in time [17], [3].

An important quantity to consider in the stability analysis of NTMs is the bootstrap current. This is a self generated current density in the plasma that is proportional to the radial pressure gradient. It can be expressed as

$$j_{\mathrm{bs}} = \frac{\sqrt{\varepsilon}}{B_\theta}\left(\frac{-\mathrm{d}p}{\mathrm{d}r}\right) \tag{2.52}$$

in the large aspect ratio approximation mentioned earlier [17].

When it comes to the magnetic islands, the evolution of perturbed bootstrap current can become more relevant as a driver of island growth. The reason being that when magnetic islands appear, the pressure profile is flattened across the island which reduces the bootstrap current inside the island. This reduction in bootstrap current is destabilising and promotes island growth [5].

An important observation to make about the instabilities of interest in this project is that they form on rational surfaces. Meaning flux surfaces where the safety factor is expressed as a ratio of two integer. To understand this we can examine a perturbation of the form

$$\psi_1 = Ae^{i\mathbf{k}\cdot\mathbf{r}} = Ae^{i(m\theta - n\phi)}. \tag{2.53}$$

The wave vector for this perturbation in the cylindrical system is given by

$$\mathbf{k} = (0, m/r, n/R). \tag{2.54}$$

If the wave vector of a perturbation is parallel to the equilibrium field it will experience restoring forces by the equilibrium field and thus be suppressed. This means that for a perturbation to grow, the condition

$$\mathbf{k} \cdot \mathbf{B} = 0 \tag{2.55}$$

has to be fulfilled [6]. The equation (2.55) can be expressed in this particular case as

$$\mathbf{k} \cdot \mathbf{B} = \frac{m}{r} B_\theta - \frac{n}{R} B_\phi = 0. \tag{2.56}$$

Using the expression of the safety factor given by equation (2.24) this equation becomes

$$\frac{B_\theta}{r} (m - nq) = 0. \tag{2.57}$$

Thus the condition $q = m/n$ results in instabilities being able to form at rational surfaces.

2.4 Tearing modes

2.4.1 Linear tearing modes and linear stability

The tearing mode instability is a complex phenomenon. But one can learn much about it with the study of the ideal plasma far away from the tearing layer. In this regime, the momentum equation (2.3) loses the plasma acceleration term since this is equilibrium and thus we only consider the force balance equation (2.8). Furthermore, since we are considering the plasma far away from the tearing layer the plasma resistivity is also negligible and equation (2.47) is the version of Ohm's law we consider.

In general, tearing modes are driven by the radial current gradient that arises in the plasma. Current gradients and pressure density gradients provide free energy that can drive different instabilities to grow. The following derivation is known [17] but

it is instructive and the resulting equation is central to this project so we go through it here as well. We begin by taking the curl of the force balance equation giving us

$$\nabla \times \mathbf{j} \times B = 0. \tag{2.58}$$

Using the curl identity

$$\nabla \times (\mathbf{j} \times \mathbf{B}) = ((\nabla \cdot \mathbf{B}) + \mathbf{B} \cdot \nabla)\,\mathbf{j} - ((\nabla \cdot \mathbf{j}) + \mathbf{j} \cdot \nabla)\,\mathbf{B} \tag{2.59}$$

and remembering that the magnetic field and the current density field are divergence free we obtain

$$\mathbf{B} \cdot \nabla \mathbf{j} - \mathbf{j} \cdot \nabla \mathbf{B} = 0. \tag{2.60}$$

The magnetic field and current density can be linearized according to $\mathbf{B} = \mathbf{B}_0 + \mathbf{B}_1$ and $\mathbf{j} = \mathbf{j}_0 + \mathbf{j}_1$. A product of two linearized quantities is negligible ($\mathbf{B}_1 \cdot \mathbf{B}_1 \approx \mathbf{j}_1 \cdot \mathbf{j}_1 \approx \mathbf{B}_1 \cdot \mathbf{j}_1 \approx 0$).

Considering the quantity orderings in equations (2.44), (2.45), (2.46) and inserting the into the toroidal direction of equation (2.60) one sees that

$$\mathbf{j}_0 \cdot \nabla \mathbf{B}_{\phi 1} \ll \mathbf{B}_0 \cdot \nabla \mathbf{j}_{\phi 1}. \tag{2.61}$$

With this information, the equation governing the region far from the tearing layer becomes

$$\left(\mathbf{B} \cdot \nabla \mathbf{j}_\phi\right)_1 = (\mathbf{B}_0 \cdot \nabla)\mathbf{j}_{\phi 1} + (\mathbf{j}_{\phi 0} \cdot \nabla)\mathbf{B}_1 = 0. \tag{2.62}$$

The perturbed helical flux $\psi(r, \theta, \phi)$ appropriate for this geometry is defined by

$$B_{r1} = -\frac{1}{r}\frac{\partial \psi}{\partial \theta}, \tag{2.63}$$

$$B_{\theta 1} = \frac{\partial \psi}{\partial r}. \tag{2.64}$$

Using this definition of the perturbed flux and inserting it in Ampère's law (2.4) for the perturbed toroidal current density we obtain

$$\mu_0 j_{\phi 1} = \nabla^2 \psi = \frac{1}{r^2}\frac{\partial}{\partial r}\left(r\frac{\partial \psi}{\partial r}\right) + \frac{1}{r^2}\frac{\partial^2 \psi}{\partial \theta^2}. \tag{2.65}$$

Assuming the perturbations take the form $\psi(r)e^{i(m\theta-n\phi)}$ where (m, n) are the poloidal and toroidal mode numbers of the perturbation, equation (2.62) can be expressed as

$$\frac{1}{\mu_0}\left(\frac{mB_\theta}{r}-\frac{nB_\phi}{R}\right)\nabla^2\psi-\frac{m}{r}\frac{\mathrm{d}j_\phi}{\mathrm{d}r}\psi=0. \tag{2.66}$$

This can be written in terms of the safety factor given by equation (2.24). From this we obtain the second order differential equation for the perturbed helical flux

$$\frac{1}{r}\frac{\mathrm{d}}{\mathrm{d}r}\left(r\frac{\mathrm{d}\psi}{\mathrm{d}r}\right)=\frac{m^2}{r^2}\psi-\frac{\mathrm{d}j_\phi/\mathrm{d}r}{\frac{B_\theta}{\mu_0}\left(1-\frac{nq}{m}\right)}\psi=0. \tag{2.67}$$

Equation (2.67) can be solved and a radial profile for $\psi(r)$ can thus be obtained. But this equation has a singularity at the value of $q(r) = m/n$ which means that the equation has to be solved separately for the left and right side of the rational surface. The full solution of the perturbed helical flux requires solving a different set of differential equations inside of the tearing layer where resistivity and inertia start to become relevant.

The discontinuity of the outer solutions is measured by the difference in the logarithmic derivatives to the left and right side of the tearing layer located at some radial point r_s. This is usually expressed as

$$\Delta'=\left[\frac{\partial(\ln\psi(r))}{\partial r}\right]_{r\to r_s^-}^{r\to r_s^+}. \tag{2.68}$$

Here, the variables r_s^+ and r_s^- approach r_s from the left and right side of the resonant surface. The quantity Δ' is called the linear tearing stability index. In short, this parameter determines if the linear tearing mode will grow with time or shrink. If $\Delta' < 0$ then the mode is stable and the tearing layer will shrink. If $\Delta' = 0$ then the mode is marginally stable and will neither shrink nor grow as time passes. And finally, if $\Delta' > 0$ then the mode will grow.

2.4.2 Cylindrical approximation of tearing index

There is approximation of the linear tearing stability index that is often used as a first step in calculating the classical linear stability. This approximation solves for the perturbed helical flux in the absence of a plasma current with the plasma geometry being a straight cylinder. These assumptions modify equation (2.67) to

$$\frac{1}{r}\frac{\mathrm{d}}{\mathrm{d}r}\left(r\frac{\mathrm{d}\psi}{\mathrm{d}r}\right)-\frac{m^2}{r^2}\psi=0. \tag{2.69}$$

This equation is analytically solvable and has solutions $\psi \propto \alpha r^{\pm m}$ [17]. Using the definition of the tearing index given in equation (2.68) one obtains the tearing index in the cylindrical approximation to be

$$\Delta'_{\mathbf{cylindrical}} = -\frac{2m}{r_s}. \tag{2.70}$$

Additions can be made to equation (2.70) when considering the distance from the conductive wall but this is the basic form of the expression.

2.4.3 Non-linear tearing modes and non linear stability

The linear stability index is an important part of the tearing mode dynamics but it is not sufficient to model the magnetic islands that arise. Due to the fact that the linear stability index is derived by ideal MHD assumptions, it fails to capture the non-linear effects near the tearing layer. These effects come about due to the plasma resistivity (η). One of the early extensive description of the non linear growth of the tearing mode came from P. H. Rutherford (1973) [12].

2.4.4 Nonlinear effects

The magnetic diffusion equation (2.50) can be used to derive a simple first approximation to the evolution equation of the magnetic island width. To do this one must assume that the perturbed magnetic field B_r is constant across the island width. By making this assumption one can arrive at the following equation for the evolution of the magnetic island width:

$$\frac{\mathrm{d}w}{\mathrm{d}t} \simeq \frac{\eta}{2\mu_0}\Delta'(w). \tag{2.71}$$

This is a rudimentary form the Rutherford Equation (RE). But this equation is only an approximation. Here, Δ' is a function of the width and is calculated using a generalization of equation (2.68) as given by [17]

$$\Delta'(w) = \left[\frac{\partial \ln\left(\psi(r)\right)}{\partial r}\right]_{r_s - w/2}^{r_s + w/2}. \tag{2.72}$$

2.4.5 Neoclassical effects

In the toroidal geometry, the tearing mode and magnetic island dynamics are affected by the shape of the plasma. Even in the large aspect ratio approximation, toroidal effects manifest.

The full equation that will be used to evolve the magnetic island in this project is

$$g_1 \frac{\tau_r}{r_s} \frac{\mathrm{d}w}{\mathrm{d}t} = r_s \left[\Delta'_0 + \Delta'_{\mathrm{bs}} - \Delta'_{\mathrm{GGJ}} - \Delta'_{\mathrm{pol}} - \mathrm{Re}(\Delta'_w) \right]. \tag{2.73}$$

This is often called the modified Rutherford Equation (MRE) and contains the following terms. The numerical factor g_1 is a factor dependent on collisionality and will be set to 1 for tesing throught the project. The term τ_r corresponds to the local resistive diffusion time and r_s is the radial coordinate of the rational surface where the tearing mode is taking place.

On the right hand side of equation (2.73) are all the Δ' terms which have a contribution to the evolution of the magnetic island width. The term labelled Δ'_0 is the classical tearing stability index given by (2.68). This term destabilizing meaning that the island width grows for positive values of Δ'_0.

Next is Δ'_{bs} which is the term that appears due to the helically perturbed bootstrap current. This term can be expressed as

$$\Delta'_{\mathrm{bs}} = a_{\mathrm{bs}} \Delta_{\mathrm{bs0}} \frac{w}{w^2 + w_d^2} \tag{2.74}$$

with

$$\Delta_{\mathrm{bs0}} = \sqrt{\varepsilon} \beta_p \left| \frac{L_q}{L_p} \right|. \tag{2.75}$$

Here, a_{bs} is a free parameter that can be adjusted to fit experimental data, w is the island width and w_d is a parameter depending on the parallel ($\chi_\parallel$) and perpendicular ($\chi_\perp$) heat diffusivities across the island given by

$$w_d \propto \left(\frac{\chi_\perp}{\chi_\parallel} \right)^{1/4}.$$

The quantities L_p and L_q are the length scales of the pressure and safety factor. The factor β_p is the poloidal β and ε is the inverse aspect ratio.

The relevant assumption for this project is that this term is destabilising for the tearing mode. Meaning when $\Delta_{\mathrm{bs}'} > 0$ the island width gets a positive contribution and grows.

Following this, there is the Δ'_{GGJ} term which is the Glasser Green Johnson contribution. This term accounts for how the magnetic island bends the field lines surrounding the tearing layer. Usually the magnetic field is curved by the island in such a way as to give a stabilizing effect. The Δ'_{GGJ} can be expressed in different ways depending on the particular system. The general form of this term is given by

$$\Delta'_{\mathrm{GGJ}} = a_{\mathrm{ggj}}\beta_p\varepsilon^2\frac{L_q^2}{r_s|L_p|}(1-1/q^2)\frac{1}{\sqrt{w^2+0.2w_d^2}}. \tag{2.76}$$

As before, a_{ggj} is a free parameter that can be adjusted to match the data.

The final two terms of the MRE are the polarisation term Δ'_{pol} and the resistive wall term $\mathrm{Re}(\Delta'_w)$. The first arising due to a polarisation current that appears as a result of $\mathbf{E}\times\mathbf{B}$ and island rotation [8]. The second term appears as a result of a resistive reactor wall where the magnitude of induced currents depends on several parameters such as vessel radius, plasma frequency and resistive wall time [2]. These terms are important to understanding the full physics of the NTMs but will not be considered to any larger extents in this project.

An important aspect of the individual terms in equation (2.73) are the signs. The sign of each term indicates whether it is generally stabilising or destabilising for the magnetic island. As can be seen in equation (2.73) the two terms that generally promote island growth are the classical tearing index (Δ'_0) and the perturbed bootstrap current contribution (Δ'_{bs}). The rest of the terms are generally stabilising. Although this depends on different factors, sometimes the terms Δ'_{pol} or Δ'_{GGJ} be destabilising depending on the specific plasma scenarios.

3

Methods

The implementations made in this project aim to contribute to simulations of the NTM stability and evolution. Python has been the principal programming language used. Other codes used in the simulation workflows are written in several languages such as `python` and `FORTRAN 2008`. This project was conducted in collaboration with ITER and the ITER computer cluster was used for the development of code.

3.1 The European Transport Simulator

The European Transport Simulator (ETS) is a simulation workflow used by the fusion research community to model tokamak plasmas. It can be used to model the full tokamak plasma or select parts. The flexibility of this simulation tool allows for modelling of plasmas in different machines like ITER, JET and more. This project mainly uses ETS-like frameworks to simulate tearing modes in ITER scenarios.

3.1.1 Workflows

The ETS and workflows based on it are set up through the MUSCLE3 library [15]. MUSCLE3 provides the tools to set up multi-scale coupled simulations which is needed when modelling tokamak plasmas. The schematic structure of code and information flow is defined using workflows. Below is an example of a very simple workflow that illustrates the basic structure.

Figure 3.1: Simple workflow illustration consisting of three actors. The first initiates the plasma scenario, the second calculates the plasma equilibrium and the third saves data and closes the simulation correctly. The arrows represent the direction of information flow.

A workflow in the latest version of ETS (ETS6) is generally set up through a configuration file with the Multiscale Modelling and Simulation Language (MMSL). This format is read by MUSCLE3 to then set up and execute the simulation. The example in figure 3.1 show what a simple equilibrium calculation workflow might look like.

First, the plasma scenario is initiated. Data is pulled from relevant databases and the relevant profiles are prepared for the next step. Next, the information is passed through the first arrow into the equilibrium actor where the plasma equilibrium is calculated and saved into a new instance of the database. Finally, the finish actor saves the data to the database and ends the simulation.

3.1.2 Actors

Actors are the building blocks of workflows. Actors are exemplified in figure 3.1. Each box represents a separate actor. The advantage of using this setup for simulations is the modularity of the approach. Each actor is mostly independent from the rest of the actors. A given actor takes some inputs and returns some outputs. If these are provided correctly the rest of the workflow can be changed without affecting the actor itself.

Keeping the input/output consistent also allows for exchanging actors without changing the rest of the workflow. This is useful in the case one needs to test different physics models or computational methods for a given actor. Only that actor has to be altered and the rest of the workflow can stay intact.

3.1.3 IMAS

The Integrated Modelling & Analysis Suite (IMAS) is a framework that defines the data representation used in ETS simulations. It standardises the data flow inside the workflows. The IMAS conventions allow for actors within workflows to be written in different programming languages and still be compatible. This means that actors written in an interpreted language such as `python` and actors written in compiled languages such as `C` or `FORTRAN` can be run within the same workflow.

The input and output of the actor is standardised by using the interface data structures (IDS) to store the data that produced by simulations. Experimental data can also be stored in the IDS standard. The IDS structures are structures defined in the Data Dictionary (DD). Each IDS is a hierarchical data structure that contains sub-structures that store the vector and scalar quantities needed to describe plasma and device characteristics [10].

3.1.4 High Modularity Physics Simulator

A framework for running simulations that is currently in early stages of development is the High Modularity Physics Simulator (HMPS). This framework can encapsulate ETS-like workflows. The implementations made in this project have been applied in HMPS simulations. A part of the project was to run the created actor inside this workflow.

3.2 Implementations

Implementations made in this project have been mainly focused on creating an actor that integrates the perturbed helical flux according to equation (2.67). The actor was then tested first in a stand alone workflow and later inside of the HMPS framework as part of a larger workflow.

3.2.1 Calculation of Δ'

An actor was implemented to calculate the linear tearing stability index. There are several ways of calculating Δ'_0 using different approximations. The actor implemented in this project uses the perturbed helical flux profiles calculated by solving the differential equation (2.67).

This calculation assumes two symmetries in the plasma. First, the toroidal symmetry which means that the plasma profiles are invariant under rotation in the toroidal angle (ϕ). The second symmetry is about the poloidal angle (θ). This symmetry comes as the result of taking the flux surface average of all relevant quantities. By doing that the θ-dependence is removed. This means that the Δ'_0 calculation only need profiles depending on the radial coordinate.

The calculations done adopt the solution methods found in an open source git repository [13]. This repository solves equation (2.67) using equations (2.3)-(2.7) and (2.23). This implementation uses an analytical $q-$profile and derives all other quantities from the analytical relations between q, B_θ, B_ϕ and j_ϕ. The code implemented in this project solves the equation using numerical input for the magnetic fields, current densities and safety factor instead. The code also implements flux surface averaging of 2-dimensional profiles.

Therefore, preprocessing is required to interpolate the profiles in an appropriate manner. Since different profiles in the IDS can have a different grids issues can arise when performing calculations. To remedy this, the profiles were interpolated using a cubic spline. After interpolation the profiles could be expressed in terms of a common grid such as the normalized toroidal flux coordinate named `rho_tor_norm`. This flux coordinate is given by

$$\texttt{rho\_tor\_norm} = \frac{\rho_{\text{tor}}}{\rho(a)} \tag{3.1}$$

where ρ_{tor} is the toroidal flux coordinate and $\rho(a)$ is the toroidal flux at the edged of the plasma.

Next, the setup for solving equation (2.67) was built. The function `solve_bvp` from the python library `scipy.integrat` was used [16]. This python function solves higher order ordinary differential equations by taking an equivalent system of first order differential equations as input. For equation (2.67) one can write the equivalent system as

$$\begin{aligned}
\psi &\equiv y_1, \\
\frac{d\psi}{dr} &= y_1' \equiv y_2, \\
\frac{d^2\psi}{dr^2} &= y_2' = \left(\frac{m^2}{r^2} + \frac{\mathrm{d}j_\Phi/\mathrm{d}r}{\frac{B_\theta}{\mu_0}\left(1 - \frac{nq}{m}\right)} \right) y_1 - \frac{y_2}{r}.
\end{aligned} \tag{3.2}$$

With this system of first order equations the only thing left to do is to calculate at each radial coordinate the factor

$$c(r) \equiv \left(\frac{m^2}{r^2} + \frac{\mathrm{d}j_\Phi/\mathrm{d}r}{\frac{B_\theta}{\mu_0}\left(1 - \frac{nq}{m}\right)} \right) \tag{3.3}$$

as well as to set the boundary conditions. Since the differential equation is of second order, there are two boundary conditions required. Moreover, this differential equation was solved separately for the plasma to the left of the resonant surface and the right. This needed to be done since equation (2.67) has a singularity at $q(r) = \frac{m}{n}$.

Inside of the differential equation solver, an internal grid was defined which was why the input profiles were interpolated with respect to `rho_tor_norm`. The concatenation of the inner solution and outer solution gives the full perturbed helical flux for our system. And with that, one sets the perturbed magnetic fields according to equations (2.63) and (2.64).

After these calculation were made, the resulting data was stored in the `mhd_linear` IDS. The linear tearing index was also calculated from the solution $\psi(r)$ according to

$$\Delta' = \frac{\psi'(r_\mathrm{s} + 10^{-8}) - \psi'(r_\mathrm{s} - 10^{-8})}{\psi(r_\mathrm{s})} \tag{3.4}$$

where r_s is the radial coordinate of the rational surface. This calculation of Δ' is done according to equation (2.68). Later implementations will need to be generalized to equation (2.72) but for this project equation (2.68) is sufficient.

This is a discretized version of equation (2.68). The choice of infinitesimal value $\varepsilon = 10^{-8}$ to the left and right of the rational surface was arbitrary. The important part in this choice was to get close to the tearing layer.

To solve this differential equation, a first guess of the solution has to be made. The guess used throughout this project was simply a straight line connecting the bound-

ary condition at the plasma centre with the boundary condition at the resonant surface for the inner solution. Likewise a straight line connecting the boundary condition at the tearing layer with the boundary condition at the edge. The boundary conditions were taken to be

$$\psi(0) = \psi(L) = 0,$$
$$\psi(r_s) = 1,$$

where L denotes the maximum value of the minor radius which in the case of normalized flux coordinates is $L = 1$. Given this the first guess of the left side solution becomes

$$\psi_{\text{left}}(r) = \frac{\psi(r_s)}{r_s} r, \quad r \in [0, r_s] \tag{3.5}$$

and the guess for the right side solution becomes

$$\psi_{\text{right}}(r) = \frac{\psi(r_s)}{r_s - 1} r + \frac{\psi(r_s)}{1 - r_s}, \quad r \in [r_s, 1]. \tag{3.6}$$

An example of this first guess can look like the following:

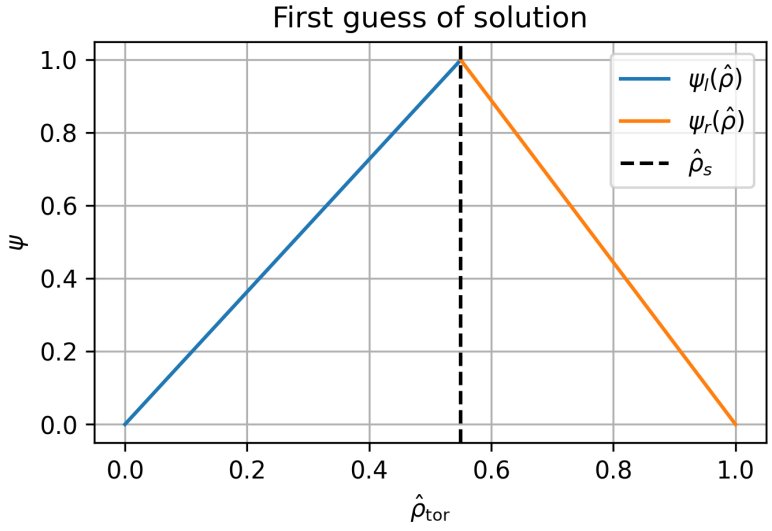

Figure 3.2: First guess of solution for perturbed helical flux. Two separate guesses are made, one to the left of the singular (tearing) layer and one to the right of it.

3.2.2 Implemented actor

The code for calculating Δ'_0 was implemented in a separate script as a single callable function. This function takes as input the radial grid `rho_tor_norm` here denoted

as ρ for simplicity, the safety factor profile $q(\rho)$, the poloidal magnetic field $B_\theta(\rho)$, the toroidal current density $j_\phi(\rho)$, the poloidal and toroidal mode numbers of the tearing mode (m, n), and finally the value of the perturbed helical flux at the rational surface $\psi(\rho_s)$ as a boundary condition.

After this, all profiles are interpolated with respect to the input grid. This is done in order to use the `solve_bvp` function with a different internal grid. The interpolation made is a cubic spline taken from the `scipy.interpolate` [16].

The value of the radial coordinate of the tearing layer is found by numerically solving for $\rho = \rho_s$ in the equation

$$\left(1 - \frac{n}{m}q = 0\right) \Leftrightarrow q(\rho) = \frac{m}{n}. \tag{3.7}$$

After this is done, the inputs to `scipy.integrate.solve_bvp` are ready according to (3.2). The produced output is then discretised back into the original input grid and returned. The linear tearing stability index is directly calculated from the output values of $\psi'_{\text{left}}(\rho)$ and $\psi'_{\text{right}}(\rho)$ according to (3.4).

The procedure described above is called as a single function from the `helical_flux.py` actor. It takes `rho_tor_norm`, j_ϕ, B_θ, q, m and n as inputs. It then returns the perturbed helical flux and Δ'_0 value. Finally the actor stores the perturbed helical flux to the `mhd_linear` IDS.

4

Results

4.1 Input scenario

The results from this project use a specific plasma scenario in all simulations. Three profiles from the plasma equilibrium are used to solve equation (2.67). The profiles are the toroidal current density j_ϕ, the safety factor q and the poloidal magnetic field B_θ.

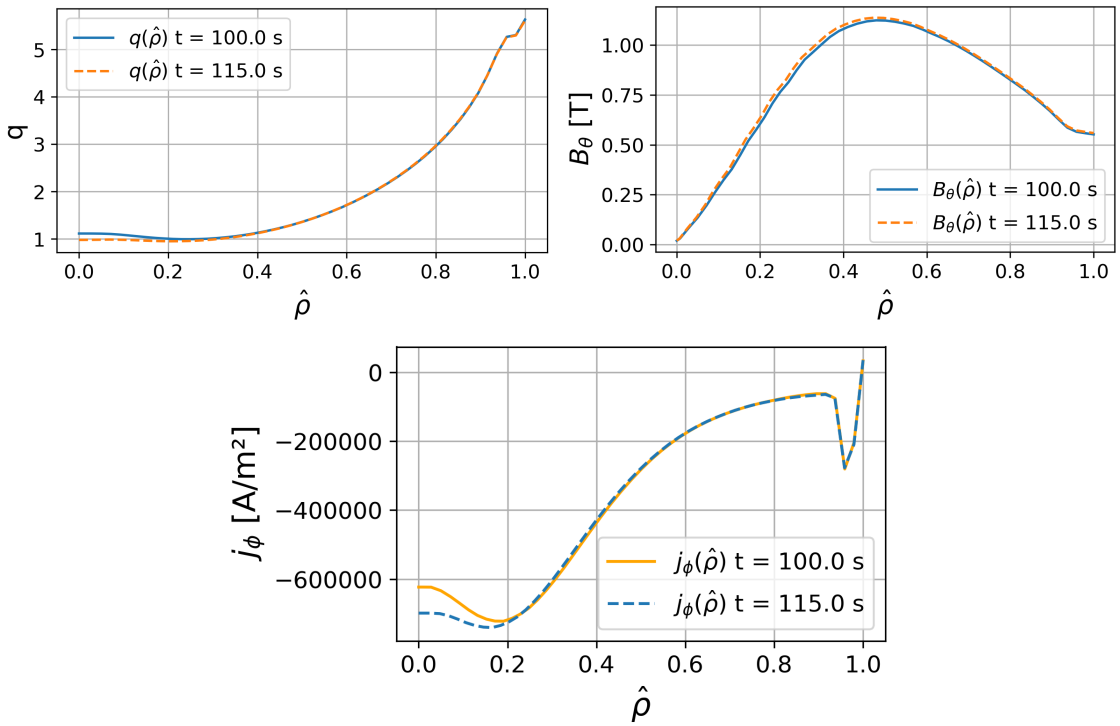

Figure 4.1: Equilibrium profiles used for calculation of the perturbed helical flux. All profiles are expressed in terms of the normalized toroidal flux coordinate ($\hat{\rho}$). Each profile is shown at two time points in the plasma scenario. The first is at 110 s and the final is 115 s.

Figure 4.1 shows the relevant equilibrium profiles used from the scenario to obtain results. This plasma scenario has an equilibrium that does not change substantially

with time although the profiles do fluctuate. This fact can be seen in the example time points plotted for each profile in the figure.

4.2 Linear tearing stability index

The main result from this project is the calculation of the linear tearing stability index (Δ'_0) given numerical equilibrium profiles of the magnetic fields, the safety factor and the current densities as input. The produced values of Δ'_0 are compared to values calculated using the cylindrical approximation as described in chapter 2.4.2.

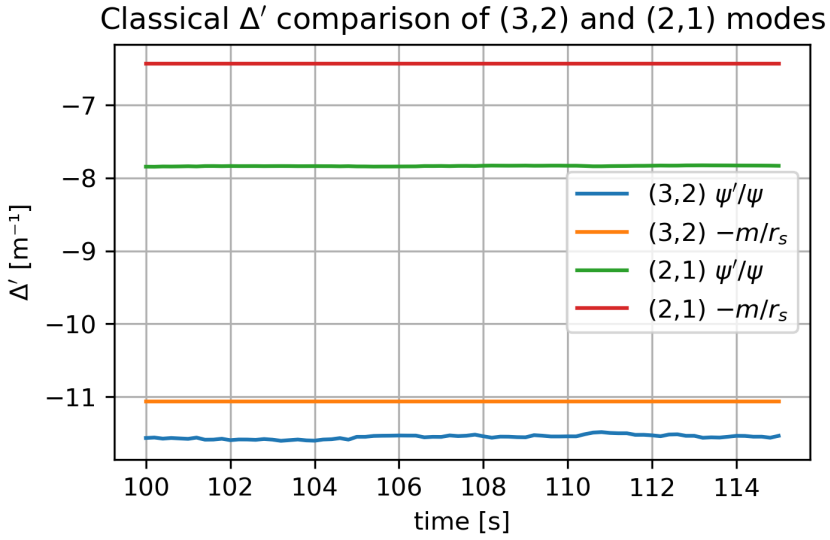

Figure 4.2: Comparison of classical tearing index calculated using cylindrical approximation to calculate Δ'_0 versus the full solution to the perturbed helical flux to calculate Δ'_0. The calculations are done for the (3,2) mode and (2,1) mode respectively.

Figure 4.2 shows how the different methods of calculating the classical tearing index give different results. The cylindrical approximation gives a constant value of Δ'_0 for each mode while the calculation via the perturbed helical flux profile gives a varying Δ'_0 in time. The fluctuation of Δ'_0 is stronger for the (3,2) tearing mode relative to the (2,1) mode. The results in figure 4.2 indicate that the tearing mode is stable in both cases. The results from the full ψ integration give more stable modes than the cylindrical approximation.

A closer look at each individual mode is also informative.

The figures 4.3 and 4.4 show how the cylindrical approximation of Δ'_0 compares to Δ'_0 as calculated via the perturbed helical flux. The modes considered are the $(m, n) = (2, 1)$ and $(3, 2)$ respectively.

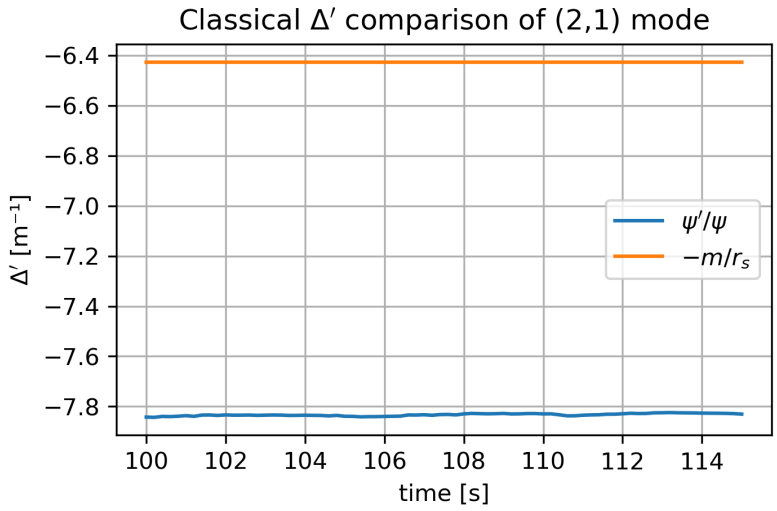

Figure 4.3: Comparison of the classical tearing index for the (2,1) tearing mode.

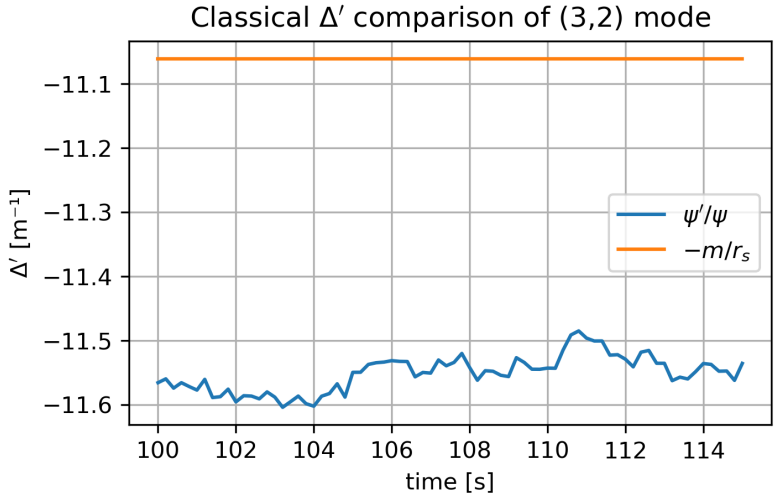

Figure 4.4: Comparison of the classical tearing index for the (3,2) tearing mode.

4.3 Contributions to island width evolution

Using existing MRE code, the different contributions to the modified Rutherford equation can be plotted. The simulations for this island evolution uses the HMPS framework.

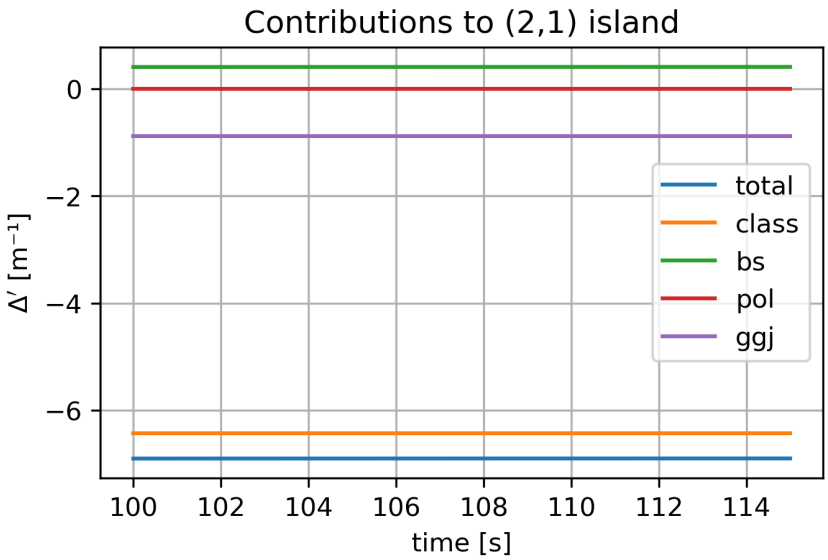

Figure 4.5: Different Δ' contributions to the island evolution width of the (2,1) tearing mode.

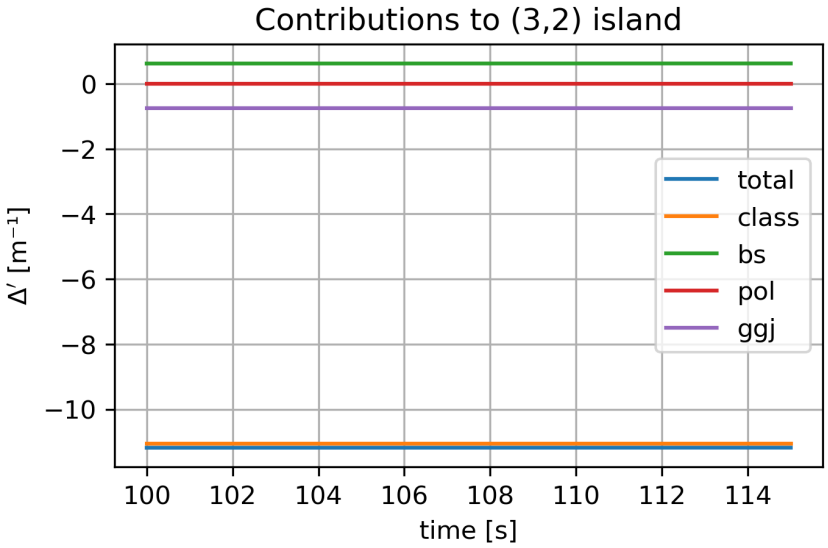

Figure 4.6: Different Δ' contributions to the island evolution width of the (3,2) tearing mode.

5

Conclusion

5.1 Understanding of tearing index results

The results described in chapter 4 are preliminary. The main work in this thesis has been focused on theoretical understanding of the NTMs along with the developments made of the perturbed helical flux actor as well as making it compatible with running in the HMPS framework. The results produced are thus not to be taken as physical, but rather as indicators showing if the simulations are on the right track.

So what can be concluded from the produced results? As can be seen in figure 4.2 the $(3, 2)$ mode give a more stable Δ'_0 than the $(2, 1)$ mode. This is to be expected given tearing mode theory. Higher poloidal mode numbers correspond to a more negative tearing stability index. This is true for the cylindrical approximation as well as for the calculation via perturbed helical flux. That in itself is an indication that the helical flux actor is on the right track.

Furthermore, one can compare how the Δ'_0 calculations differ between the cylindrical approximation and the numerically calculated one. In figure 4.3 the stability index calculated according to the cylindrical approximation is constant in time. This is reasonable since the cylindrical approximation does not take into account any plasma profiles according to equation (2.70). In contrast to this, the tearing index calculated via the perturbed helical flux integration fluctuates. This is possibly explained by the fact that at each time step the input equilibrium profiles are different since the equilibrium is not completely static in time. That results in a variation of Δ'_0. To quantify this we can compare how the equilibrium current density gradient fluctuates for the different modes. Fluctuations of the current density gradient at the resonant surface can be measure by the relative fluctuation given as

$$F(j'_{\phi(m,n)}) \equiv \left. \frac{\delta j'_\phi}{\left\langle j'_\phi \right\rangle} \right|_{(m,n)} . \tag{5.1}$$

Here, $\delta j'_\phi$ is the standard deviation of the toroidal current gradient at the resonant surface and $\left\langle j'_\phi \right\rangle$ is the time averaged toroidal current gradient at the resonant

surface. This measure by itself is difficult to interpret so we take the ratio of the relative fluctuation of the (3,2) mode to the relative fluctuation of the (2,1) mode.

For the scenario used in the time span $110\,\mathrm{s} - 115\,\mathrm{s}$ we obtain

$$\frac{F(j'_{\phi(3,2)})}{F(j'_{\phi(2,1)})} = 1.33. \tag{5.2}$$

The result in equation (5.2) indicates that the (3,2) tearing mode has higher relative fluctuations for j'_ϕ near the resonant surface compared to the (2,1) mode. This could explain the more violent fluctuations in Δ'_0 in figure 4.4 compared to figure 4.3.

When it comes to the $(3, 2)$ tearing index seen in figure 4.4 one sees similar properties. Although here, the variations in Δ'_0 are larger than for the $(2, 1)$ mode. This can be quantified by the standard deviation of the the different Δ'_0 values.

Table 5.1: Comparison of two ways of calculating the stability tearing index for the $(2, 1)$ and $(3, 2)$ tearing modes.

(m, n)	$\Delta'_{\text{cylinder}}$	average Δ'_0	standard dev. Δ'_0
$(2, 1)$	$-6.43\,\mathrm{m}^{-1}$	$-7.83\,\mathrm{m}^{-1}$	$0.005\,\mathrm{m}^{-1}$
$(3, 2)$	$-11.06\,\mathrm{m}^{-1}$	$-11.55\,\mathrm{m}^{-1}$	$0.027\,\mathrm{m}^{-1}$

Table 5.1 shows the average value of Δ'_0 from the numerical integration of ψ. The standard deviation gives a measure of how much the tearing index varies in time. The values for standard deviation in both modes show small variation in comparison to the mean values. For the (2,1) mode the standard deviation is 0.06% of the mean and for the (3,2) mode it is 0.2% of the mean.

5.2 Understanding of modified Rutherford equation results

As can be seen from both figures 4.5 and 4.6 Δ'_0 does not evolve much in time. This is due to the fact that the tearing modes in the plasma scenario used are stable. In both results the stability contribution from the classical tearing index and the curvature term far outweighs the destabilising contribution from the perturbed bootstrap current. Thus, the islands should simply vanish for this particular scenario.

In these result we can see how the different terms contribute to the NTM. It is interesting to note which terms contribute to the NTM instability and which terms suppress the NTM. In both the $(2, 1)$ and $(3, 2)$ tearing modes the main driver of the island growth is the perturbed bootstrap current term (Δ'_{bs}). But this term is not enough to drive the island to grow according to (2.73). The classical tearing index (Δ'_0) combined with the stabilising curvature term (Δ'_{GGJ}) suppress the modes to much for any growth to occur.

5.3 Reflection on implementations

The implementation of the helical flux actor took an existing code that implemented calculations of analytical profiles and turned it into a solver that can take in numerical profiles as input and calculate the perturbed helical flux from that. The helical flux actor also implemented a basic version of flux surface averaging. The resulting linear tearing index gives a more physical result based on the input profiles rather than the simpler cylindrical model. The cylindrical tearing index may be a candidate as an upper limit for the value of Δ_0' since it gives the least stable tearing index value for this plasma scenario.

A big part of the implementation was making the input and output compatible with the framework and workflow of ETS and HMPS. This required much trial and error due to the complexity of these workflows. Although the goal of the HMPS is to have a more robust interface when inserting different actors into the workflow, the development phase is one where many adjustments need to be made in order to test and debug.

5.4 Outlook

Future work and development is needed to obtain physically sound simulations that can be used in realistic plasma scenarios. The next steps should be to check the boundary conditions chosen for the solution of the perturbed helical flux.

The Δ_0' actor should be integrated with the modified Rutherford equation code and coupled with the case when ψ is calculated numerically.

Island frequency also contributes to the width evolution which needs be part of the full MRE model. This will require coupling of the differential equations governing island rotation with the polarization term in equation (2.73). Development on actors for this calculation and integrating these actors in simulation workflows such as the ETS or HMPS is an important step in future developments.

The coupling of island seeding events such as sawtooth crashes to the MRE code will also be important for predicting how the plasma will behave in realistic scenarios.

One of the further goals is to connect the island evolution with transport in the plasma. For this, extension of the model need to be modified and further developed in order to use it with the predictive mode of the workflow evolving the kinetic properties consistently.

Bibliography

[1] INTERNATIONAL ATOMIC ENERGY AGENCY. *Fusion Energy*. https://www.iaea.org/bulletin/62-2. Accessed: 2025-09-25. May 2021.

[2] V Basiuk, P Huynh, A Merle, S Nowak, O Sauter, JET Contributors, and the EUROfusion-IM Team. "Towards self-consistent plasma modelisation in presence of neoclassical tearing mode and sawteeth: effects on transport coefficients". In: *Plasma Physics and Controlled Fusion* 59.12 (Nov. 2017), p. 125012. DOI: 10.1088/1361-6587/aa8c8c. URL: https://dx.doi.org/10.1088/1361-6587/aa8c8c.

[3] Paul M. Bellan. *Fundamentals of Plasma Physics*. Cambridge University Press, 2006.

[4] EUROfusion. *Fusion History Timeline*. https://euro-fusion.org/fusion/history-of-fusion/. Accessed: 2025-09-25.

[5] R. Fitzpatrick, Rajesh Maingi, Jong-Kyu Park, and Steve Sabbagh. "Theoretical investigation of the triggering of neoclassical tearing modes by transient resonant magnetic perturbations in NSTX". In: *Physics of Plasmas* 30.7 (July 2023), p. 072505. DOI: 10.1063/5.0155038. eprint: https://pubs.aip.org/aip/pop/article-pdf/doi/10.1063/5.0155038/18034120/072505_1_5.0155038.pdf. URL: https://doi.org/10.1063/5.0155038.

[6] Richard Fitzpatrick. *Magnetic Reconnection in Tokamaks*. https://farside.ph.utexas.edu/talks/peking.pdf. Institute for Fusion Studies University of Texas at Austin Austin TX, USA. 2011.

[7] Jeffrey P. Freidberg. *Ideal MHD*. Cambridge University Press, 2014.

[8] R. Haye. "Neoclassical tearing modes and their control". In: *Physics of Plasmas* 13 (May 2006), pp. 055501–055501. DOI: 10.1063/1.2180747.

[9] Richard Hazeltine and Michael Montgomery. "On tokamak equilibrium". In: *Journal of Plasma Physics* 40 (Dec. 1988), pp. 481–491. DOI: 10.1017/S0022377800013453.

[10] ITER Organization. *IMAS Data Dictionary documentation Version 4.0.0-324-g5180c82*. https://imas-data-dictionary.readthedocs.io/en/latest/index.html. 2025.

[11] J. Loizu and D. Bonfiglio. "Nonlinear saturation of resistive tearing modes in a cylindrical tokamak with and without solving the dynamics". In: *Journal of Plasma Physics* 89.5 (2023), p. 905890507. DOI: 10.1017/S0022377823000934.

[12] P. H. Rutherford. "Nonlinear growth of the tearing mode". In: *The Physics of Fluids* 16.11 (Nov. 1973), pp. 1903–1908. ISSN: 0031-9171. DOI: 10.1063/1.

1694232. eprint: https://pubs.aip.org/aip/pfl/article-pdf/16/11/1903/12262797/1903_1_online.pdf. URL: https://doi.org/10.1063/1.1694232.

[13] EPFL (jeremy.salm@epfl.ch) Salm Jérémy. *tm_solver*. https://github.com/jeremslm/Tearing_Mode_Solver/tree/main.

[14] O. Sauter and S.Yu. Medvedev. "Tokamak coordinate conventions: COCOS". In: *Computer Physics Communications* 184.2 (2013), pp. 293–302. ISSN: 0010-4655. DOI: https://doi.org/10.1016/j.cpc.2012.09.010. URL: https://www.sciencedirect.com/science/article/pii/S0010465512002962.

[15] Lourens E. Veen and Alfons G. Hoekstra. "Easing Multiscale Model Design and Coupling with MUSCLE 3". In: *Computational Science – ICCS 2020*. Ed. by Valeria V. Krzhizhanovskaya, Gábor Závodszky, Michael H. Lees, Jack J. Dongarra, Peter M. A. Sloot, Sérgio Brissos, and João Teixeira. Cham: Springer International Publishing, 2020, pp. 425–438. ISBN: 978-3-030-50433-5.

[16] et. al. SciPy 1.0 Contributors Virtanen. "SciPy 1.0: Fundamental Algorithms for Scientific Computing in Python". In: *Nature Methods* 17 (2020), pp. 261–272. DOI: 10.1038/s41592-019-0686-2. URL: https://doi.org/10.1038/s41592-019-0686-2.

[17] John Wesson. *Tokamaks*. Third. Oxford Science Publications, 2004.

DEPARTMENT OF SPACE, EARTH AND ENVIRONMENT
CHALMERS UNIVERSITY OF TECHNOLOGY
Gothenburg, Sweden
www.chalmers.se

CHALMERS
UNIVERSITY OF TECHNOLOGY